Phase diagram and multicritical behaviors of mixtures of three-dimensional bosonic gases

Giacomo Ceccarelli,[1] Jacopo Nespolo,[1,2] Andrea Pelissetto,[3] and Ettore Vicari[1]

[1]*Dipartimento di Fisica, Università di Pisa and Istituto Nazionale di Fisica Nucleare, Largo Pontecorvo 3, I-56127 Pisa, Italy*
[2]*Department of Physics, Arnold Sommerfeld Center for Theoretical Physics, and Center for Nanoscience,*
Ludwig-Maximilians-Universität München, Theresienstrasse 37, D-80333 Munich, Germany
[3]*Dipartimento di Fisica, Università di Roma "La Sapienza" and Istituto Nazionale di Fisica Nucleare, Sezione di Roma I, I-00185 Roma, Italy*

We investigate the Bose-Einstein condensation (BEC) patterns, the critical and multicritical behaviors of three-dimensional mixtures of bosonic gases with density-density interactions, characterized by a global U(1)⊕U(1) symmetry [one U(1) transformation for each species]. In particular, we consider the three-dimensional Bose-Hubbard model for two lattice bosonic gases coupled by an on-site interspecies density-density interaction. We study the phase diagram and the critical behaviors along the transition lines of the BEC of one or both species. We present mean-field calculations and finite-size scaling analyses of quantum Monte Carlo data. We also investigate the nature of the multicritical points where the BEC transition lines of the two species meet. The corresponding universality classes are inferred from a renormalization-group analysis of the corresponding multicritical U(1)⊕ U(1) Landau-Ginzburg-Wilson Φ^4 theory. We find two distinct critical behaviors, associated with bicritical and tetracritical points, respectively, depending on the relative strength of the interspecies and intraspecies interactions.

I. INTRODUCTION

The complex behavior of mixtures of bosonic gases has been extensively investigated experimentally, in particular, in cold-atom systems [1–22], and theoretically [23–50]. These systems exhibit a rich behavior, at zero and finite temperature, with several different phases separated by transition lines, along which one or more components of the system undergo Bose-Einstein condensation (BEC).

In this paper we consider three-dimensional (3D) mixtures of two different bosonic gases with short-range interactions that only depend on the local densities of the two gases. The Hamiltonian of these systems is invariant under U(1) transformations acting independently on each species, so the model is U(1)⊕ U(1) symmetric. In particular, we consider the 3D two-component Bose-Hubbard model with an on-site interspecies density-density interaction. This is a realistic model for two bosonic species in optical lattices [51].

We determine the finite-temperature phase diagram by using a variety of techniques. First, we consider the mean-field (MF) approximation, determining the qualitative phase behavior of the system as a function of the model parameters, such as the chemical potentials and the on-site interspecies and intraspecies couplings. We find several different phases, in which each species may be in the normal or superfluid state, and identify critical lines and multicritical points (MCPs) where some transition lines meet.

The 3D phase diagram is investigated in the hard-core (HC) limit of each species by a finite-size scaling (FSS) analysis of quantum Monte Carlo (QMC) simulations. The numerical data allow us to identify the universality class of the transition lines that correspond to the BEC of one of the two species. We show that, independently of whether the noncritical component is in the normal or superfluid phase, the critical behavior of the condensing species belongs to the 3D *XY* universality class characterized by the breaking of a global U(1) symmetry and by short-range effective interactions. This is the same universality class associated with the BEC of a single bosonic gas [52–55] (and also with the superfluid transition in ⁴He [56,57], with transitions in some liquid crystals characterized by density or spin waves and in magnetic systems with easy-plane anisotropy, etc. [58]). This result implies an effective decoupling of the critical modes of the condensing species from those of the noncritical component, independently of whether the latter is in the normal or superfluid phase.

The phase diagram of mixtures of bosonic gases also presents particular points where some transition lines meet. Multicritical behaviors develop at these MCPs, arising from the competition of the two U(1) order parameters associated with the BEC of the two species. To identify the possible universality classes of the multicritical behaviors, we use the field-theoretic approach, considering the effective Landau-Ginzburg-Wilson Φ^4 theory for two complex fields with global U(1)⊕ U(1) symmetry. We study the renormalization-group (RG) flow in the quartic-parameter space, identifying the stable fixed points, which control the critical behavior, and their attraction domain. We obtain accurate results from the analysis of high-order perturbative series, which are resummed taking into account their Borel summability.

The paper is organized as follows. In Sec. II we define the Bose-Hubbard model for two lattice bosonic gases. In Sec. III we determine the phase diagram of the model in the MF approximation, showing that, by changing the model parameters, one can obtain qualitatively different behaviors. In Sec. IV we present a numerical analysis based on QMC simulations in the hard-core limit and determine the critical behavior along the transition lines where one species undergoes BEC. In Sec. V we study the multicritical behaviors at the MCPs where BEC transition lines meet in the phase diagram. Finally, in Sec. VI we summarize and draw our conclusions. The Appendix reports the five-loop perturbative series in the minimal-subtraction scheme, which are used in the RG study of the multicritical behavior.

II. BOSE-HUBBARD MODEL OF A MIXTURE OF BOSONIC GASES

The two-species Bose-Hubbard (2BH) model is a lattice model appropriate to describe mixtures of bosonic gases with local density-density interactions. Its Hamiltonian reads

$$H = -\sum_{s,\langle \boldsymbol{x}\boldsymbol{y}\rangle} t_s(b^\dagger_{s\boldsymbol{x}} b_{s\boldsymbol{y}} + \text{H.c.}) - \sum_{s,\boldsymbol{x}} \mu_s n_{s\boldsymbol{x}}$$
$$+ \frac{1}{2}\sum_{s,\boldsymbol{x}} V_s n_{s\boldsymbol{x}}(n_{s\boldsymbol{x}} - 1) + U\sum_{\boldsymbol{x}} n_{1\boldsymbol{x}} n_{2\boldsymbol{x}}, \qquad (1)$$

where $\boldsymbol{x}$ is a site of a cubic lattice, $\langle \boldsymbol{x}\boldsymbol{y}\rangle$ labels a lattice link connecting two nearest-neighbor sites, the subscript s labels the two species, and $n_{s\boldsymbol{x}} \equiv b^\dagger_{s\boldsymbol{x}} b_{s\boldsymbol{x}}$ is the density operator of the s species. The 2BH model is symmetric under the U(1) transformations $b_{s\boldsymbol{x}} \rightarrow e^{i\theta_s} b_{s\boldsymbol{x}}$ independently acting on the two species. Therefore, the global symmetry group is U(1) $\oplus$ U(1).

For $t_1 = t_2$, $\mu_1 = \mu_2$, and $V_1 = V_2 = V$, the 2BH model (1) describes the behavior of a mixture of two identical bosonic gases and it has been extensively studied in Ref. [50]. In this case, the model has an additional $\mathbb{Z}_2$ exchange symmetry, so the symmetry group becomes $\mathbb{Z}_{2,e} \otimes [\text{U}(1) \oplus \text{U}(1)]$. In the HC limit, or, more generally, when $V \gtrsim U$, both components condense at the transition. Thus, the global symmetry breaks to $\mathbb{Z}_{2,e} \otimes [\mathbb{Z}_2 \oplus \mathbb{Z}_2]$. The critical behavior is controlled by a decoupled 3D XY fixed point [50]: The critical behaviors of the two gases are effectively decoupled and belong to the 3D XY universality class associated with the symmetry breaking U(1) $\rightarrow \mathbb{Z}_2$. Although the interspecies density-density interaction does not change the leading critical behavior, it plays an important role close to criticality, as it gives rise to very slowly decaying scaling corrections, which are not present at the BEC transition of a single bosonic species. In the opposite case, i.e., for $V \lesssim U$, only one component condenses, so the global symmetry is broken to U(1) $\oplus \mathbb{Z}_2$. The associated critical behavior belongs to a different 3D universality class [50].

In the following we consider mixtures of nonidentical gases described by the 2BH model (1). As we will see, their finite-temperature phase diagrams present several phases where the two species are in the normal or superfluid state, separated by transition lines along which only one species condenses. Moreover, we will discuss MCPs, which are points in the phase diagram where some transition lines meet.

The HC limit for the s component is obtained by taking $V_s \rightarrow \infty$. In this limit, using the particle-hole transformation, we can relate the spectrum of the Hamiltonian for two different sets of parameters. For instance, assume that $V_1 = \infty$ so that $n_{1\boldsymbol{x}}$ can only have the values 0 and 1. Under a particle-hole transformation the kinetic term is unchanged, while $n_{1\boldsymbol{x}} \rightarrow 1 - n_{1\boldsymbol{x}}$. Thus, the spectrum of the model with chemical potentials μ_1 and μ_2 and interaction U is related to that of the model with chemical potentials μ'_1 and μ'_2 and interaction U' with

$$\mu'_1 = -\mu_1, \quad \mu'_2 = \mu_2 - U, \quad U' = -U. \qquad (2)$$

Indeed, the energy levels of the two models differ by an irrelevant constant term proportional to μ_1. An analogous relation holds for the second species if $V_2 = \infty$. These relations imply that if one of the two components has a hard

core, one can limit oneself to study the phase diagram for $U > 0$.

III. MEAN-FIELD PHASE DIAGRAMS

Some qualitative or semiquantitative aspects of the phase diagram can be inferred by MF calculations. For this purpose we make the approximation

$$b^\dagger_{s\boldsymbol{x}} b_{s\boldsymbol{y}} = [(b^\dagger_{s\boldsymbol{x}} - \phi^*_s) + \phi^*_s][(b_{s\boldsymbol{y}} - \phi_s) + \phi_s]$$
$$\approx \phi_s b^\dagger_{s\boldsymbol{x}} + \phi^*_s b_{s\boldsymbol{y}} - |\phi_s|^2, \qquad (3)$$

where $\phi_s = \langle b_{s\boldsymbol{x}}\rangle$ are two complex space-independent variables, which play the role of order parameters at the BEC transitions. The parameters ϕ_s are related to the superfluid densities by $\rho_s \propto |\phi_s|^2$. Equation (3) allows us to rewrite the Hamiltonian (1) as a sum of decoupled one-site Hamiltonians

$$H_{\text{MF}} = -2d\sum_s t_s(\phi_s b^\dagger_s + \phi^*_s b_s - |\phi_s|^2)$$
$$- \sum_s \mu_s n_s + \frac{1}{2}\sum_s V_s n_s(n_s - 1) + U n_1 n_2, \qquad (4)$$

where $n_s = b^\dagger_s b_s$. Since the spectrum of the theory is invariant under $b_s \rightarrow e^{i\theta_s} b_s$, where the θ_s are two independent phases, the two parameters ϕ_s can be assumed to be real without loss of generality. They are determined by minimizing the single-site free energy

$$F = -T \ln\sum_i e^{-\beta E_i}, \qquad (5)$$

where E_i are the eigenvalues of H_{MF} [59]. At zero temperature the minimization of the free energy corresponds to the minimization of the ground-state energy E_0.

In the following we restrict ourselves to the case $t_1 = t_2 = t$ and $V_1 = V_2 = V$. Moreover, we set $t = 1$ so that all energies are expressed in units of t.

The model shows a complex phase diagram, with transition lines (surfaces) along which one component undergoes a transition from the normal state to a superfluid one. Note that, in the limit of zero temperature, the normal phases become Mott insulating phases or simply correspond to the vacuum. In the following we present MF results for some selected values of the model parameters, which should be representative of the different finite-temperature behaviors that can be observed by varying the parameters.

To begin with, we consider the HC limit $V \rightarrow \infty$. Figure 1 shows the zero-temperature phase diagram as a function of μ_1 and U, when component 2 has zero chemical potential, i.e., for $\mu_2 = 0$. We observe several Mott and superfluid phases, separated by continuous transition lines. The Mott phases appearing in Fig. 1 are somewhat trivial, as they correspond to the vacuum or to unit filling (one particle per site). If one chooses more general values for t_s and V_s, one may obtain more complex Mott phases at $T = 0$. For instance, for $\mu_1 = \mu_2$ and $t_1 \neq t_2$, the phase diagram also shows a Mott phase with global unit filling, i.e., $n_1 + n_2 = 1$ but $n_s \neq 0, 1$, and therefore a degenerate ground state [25]. The large degeneracy of the ground state may be described in terms of *isospin* degrees
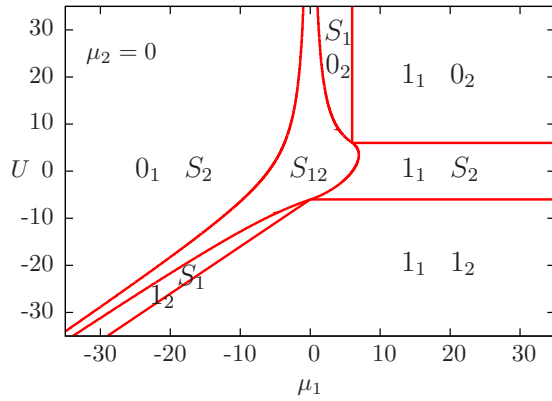
FIG. 1. The MF zero-temperature phase diagram of the 2BH model in the HC limit for $\mu_2 = 0$, as a function of μ_1 and U. The symbol S marks the superfluid phases: S_1 and S_2 indicate the phases in which only components 1 and 2 are superfluid, respectively; in phase S_{12} both components are superfluid. The symbols 0_s and 1_s mark Mott phases for species s with fillings 0 and 1, respectively. In the leftmost phase marked $0_1, S_2$, we have $\rho_2 = 1/4$ for the superfluid density and $n_2 = 1/2$, which are the values corresponding to a single gas with vanishing chemical potential.

of freedom per site, interacting by means of an effective low-energy spin Hamiltonian [25–27,31].

At finite temperature the vacuum and Mott phases are replaced by normal phases. As suggested by the $T = 0$ phase diagram of Fig. 1, we may have different behaviors depending on the strength of the interspecies interaction U. For example, Fig. 2 shows the phase diagram for $\mu_2 = 0$ as a function of μ_1 and T, for two values of U, $U = 10$ and $U = 4$. For $U = 10$ there is a single MCP where four transition lines meet. For $U = 4$ instead two different MCPs are present. The change of behavior occurs for $U = 6$. It can be related to the phase boundary $U = 2d$ appearing in the phase diagram of a single HC bosonic gas. In the MF approximation all phase boundaries correspond to continuous transitions.

In order to understand the role of finite intraspecies couplings, we consider a finite V. In this case, Mott phases with higher integer fillings are possible. Moreover, when $V < U$ one may have first-order transition lines between the superfluid phases of the two components. For example, Fig. 3 shows the zero-temperature behavior for $\mu_2 = 0$ and $U = 4$ as a function of V and μ_1. In this case, the phase S_1, in which component 1 is superfluid and component 2 is depleted, is separated from phase S_2, in which component 2 is superfluid and component 1 is depleted, by a first-order transition line with $\mu_1 = 0$ and $0 < V < U$.

Finite intraspecies interactions lead to significant changes of the phase diagram also at finite temperature. For example, Fig. 4 shows the phase behavior for $U = 4$, $\mu_2 = 0$, and some finite values of V, as a function of μ_1 and T. It should be compared with Fig. 2, where we report the phase diagram in the HC limit for the same values of U and μ_2. As V is increased from $V = 34.8$ to $V = 35.3$, the phase diagram changes qualitatively. For $V \lesssim 35$ only one MCP is present, while for $V \gtrsim 35$ three MCPs occur. Moreover, for $V \approx 35.3$ there are two different S_{12} phases. In particular, both components condense for any $\mu_1 \gtrsim 17$, if T is not too large.
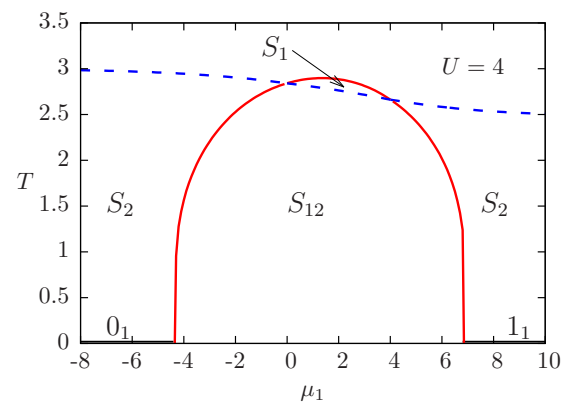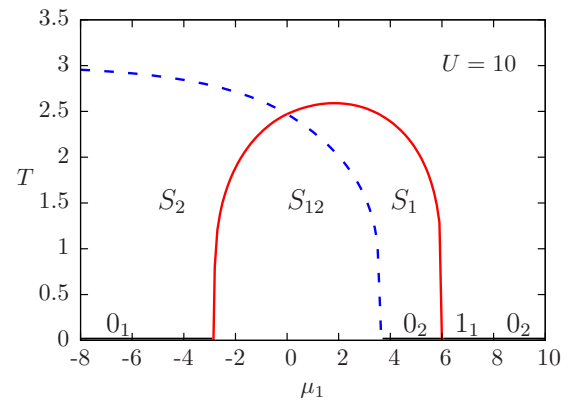

FIG. 2. Phase diagram of the HC 2BH model for $\mu_2 = 0$ and two values of U, $U = 10$ (top) and $U = 4$ (bottom), as a function of μ_1 and T. In phase S_1 component 1 is in the superfluid state, while component 2 is in the normal state. In phase S_2 the opposite occurs. In phase S_{12} both gases are superfluid. In the upper (and, for $U = 10$, rightmost) region with no label both gases are in the normal state. The solid and dashed lines indicate the normal-to-superfluid transition lines of gases 1 and 2, respectively.

Such a large-μ_1 S_{12} phase occurs for any finite V: For μ_1 larger than a V-dependent value $\mu_b(V)$, i.e., for $\mu_1 \gtrsim \mu_b(V)$, both components always condense for small T. For $V \to \infty$ we have $\mu_b(V) \to \infty$, so such a phase does not exist in the HC case, as shown in the bottom panel of Fig. 2.
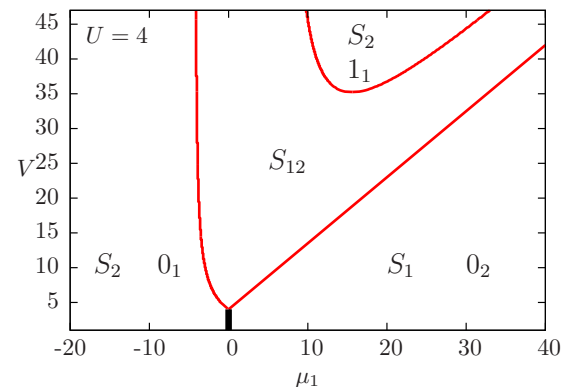

FIG. 3. Zero-temperature phase diagram for $\mu_2 = 0$ and $U = 4$, as a function of μ_1 and V. The different phases are labeled as in Fig. 1. For $V < U = 4$, a first-order transition line (indicated by a thick line) runs along $\mu_1 = 0$. The phase $1_1, S_2$ occurs only for $V \gtrsim 35.3$.
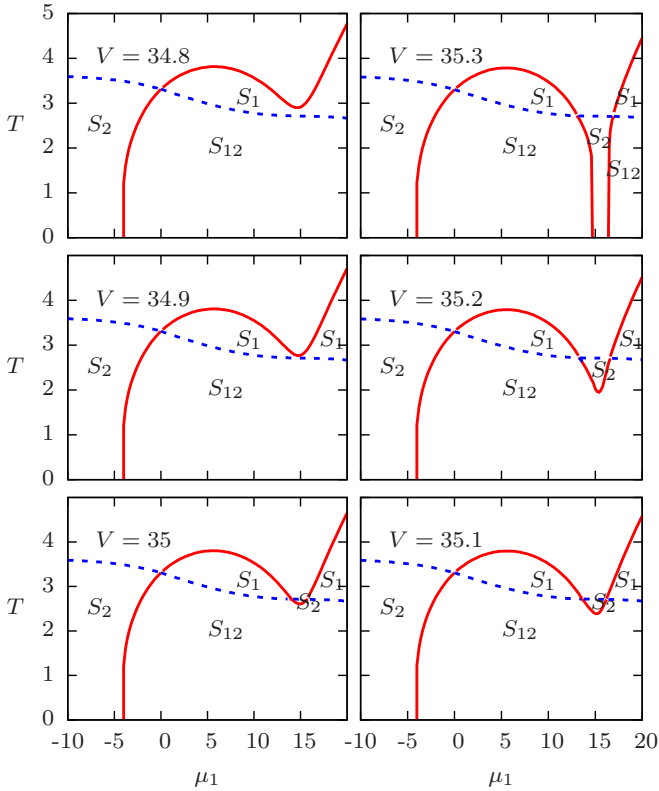
FIG. 4. Phase diagrams for $\mu_2 = 0$ and $U = 4$ as a function of T and μ_1. We report results for several values of the intraspecies repulsion V, for V close to $V \approx 35$ [at $T = 0$, the phase $1_1, S_2$ occurs only for $V \gtrsim 35.3$ (see Fig. 3)]. The different phases and the transition lines are labeled as in Fig. 2.

When $V < U$ the finite-temperature phase diagram changes significantly from that observed in the regime $V > U$. Indeed, as shown in Fig. 5, in the phase diagram for $\mu_2 = 0$, $V = 5$, and $U = 10$, three transition lines meet at a MCP: two continuous
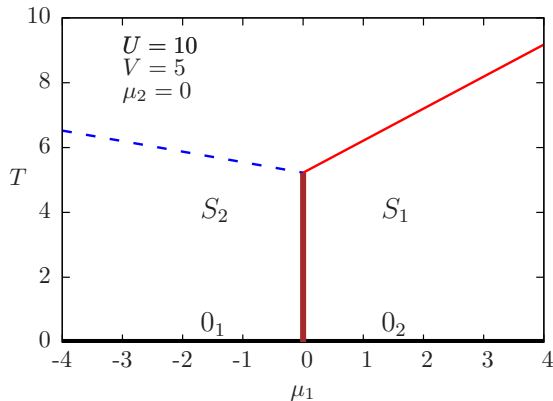

FIG. 5. Phase diagram for $\mu_2 = 0$, $U = 10$, and $V = 5$, as a function of μ_1 and T. Species 1 and 2 are superfluid for $\mu_1 > 0$ and $\mu_1 < 0$, respectively. These phases are separated by a first-order transition line along $\mu_1 = 0$, ending at the point where the continuous normal-to-superfluid transition lines of the two gases meet. In the uppermost phase with no labels, both components are in the normal state.

normal-to-superfluid transition lines and a first-order transition line separating the superfluid phases of gases 1 and 2 along the line $\mu_1 = 0$. This is of course consistent with what is observed at zero temperature (see Fig. 3).

Mean-field calculations can be straightforwardly extended to more general cases, such as $V_1 \neq V_2$ and/or $t_1 \neq t_2$. However, the main features of the possible finite-temperature behaviors should already be present in the results shown above.

IV. PHASE DIAGRAM IN THE HARD-CORE LIMIT

In this section we investigate numerically the nature of the transitions occurring in two-component bosonic systems described by the Hamiltonian (1), by QMC simulations. As already discussed in the MF approximation, in most of the cases the transition lines are associated with normal-to-superfluid transitions of one of the two species. However, it is also possible to have first-order transition lines between two phases in which only one component is superfluid [this behavior is expected in the soft-core regime (see Fig. 5)] and MCPs where three or four transition lines meet.

Since the normal-to-superfluid transition of a single species is related to the spontaneous breaking of the U(1) symmetry of the condensing species, it seems natural that the critical behavior belongs to the standard 3D XY universality class [58]. This conjecture, however, requires that the second (spectator) component plays no role at the transition, i.e., an effective decoupling of the critical modes of the condensing species from the modes of the spectator one. This hypothesis is quite natural when the spectator species is in the normal phase, which is characterized by short-range correlations. However, if the second component is in the superfluid phase, in which long-range spin-wave (Goldstone) modes develop, the asymptotic decoupling of the two species is no longer obvious. Indeed, the Goldstone modes may give rise to effective long-range interactions among the condensing particles. As a consequence, one might observe a different critical behavior (we recall that the standard 3D XY universality is observed only if the interactions decay sufficiently fast with the distance), or XY behavior with peculiar slowly decaying scaling corrections, as it occurs in the case of mixtures of identical bosonic gases [50].

To investigate these issues, we perform QMC simulations of the 2BH model in the HC limit for both species ($V_1 = V_2 \to \infty$). Our results provide robust evidence that the critical behaviors belong to the 3D XY universality class along all continuous transition lines, including those where one species condenses in the superfluid background of the other one. In other words, the local interspecies density-density interaction is an irrelevant RG perturbation at all BEC transition lines. There is also no evidence of slowly decaying scaling corrections. Apparently, the leading scaling corrections are always controlled by the leading irrelevant RG operator that appears in the standard XY model or at the BEC transition of a one-component bosonic gas.

As we will see in Sec. V, these features change when we approach a MCP, where several transition lines meet. In that case the competition of the two BEC order parameters gives rise to more important effects.

A. Quantum Monte Carlo simulations

We consider the 2BH model (1) with $t_1 = t_2 = t = 1$ in the HC limit $V_1, V_2 \rightarrow \infty$, for cubic L^3 lattices with periodic boundary conditions. We perform QMC simulations [60,61] for $\mu_2 = 0$ and two values of U, $U = 10$ and $U = 4$, using the same algorithm employed in Ref. [50] (we refer to this reference for technical details). In the MF approximation, the phase behavior as a function of T and μ_1 is reported in Fig. 2. Here we verify that the MF diagram is qualitatively correct. Moreover, we determine the nature of the critical behavior at a few selected points, at which the spectator species is both in the normal and in the superfluid phase.

For this purpose, we focus on the FSS behavior of the helicity modulus, which generally provides the most precise numerical results to characterize the critical behavior. The helicity modulus Υ_s of species $s = 1,2$ is obtained from the response of species s to a twist in the boundary conditions by an angle α_s, i.e.,

$$\Upsilon_s \equiv -\frac{1}{L} \left. \frac{\partial^2 \ln Z(\alpha_s)}{\partial \alpha_s^2} \right|_{\alpha_s = 0}, \qquad (6)$$

where $Z(\alpha_s)$ is the partition function for twisted boundary conditions in one direction and periodic boundary conditions in the two orthogonal directions. In QMC simulations Υ_s is simply related to the linear winding number W_s of species s, through the relation $\Upsilon_s = \langle W_s^2 \rangle / L$.

We also computed expectation values of other observables, such as the two-point function $\langle b_{\mathbf{sx}}^\dagger b_{\mathbf{sy}} \rangle$, its spatial integral, and the second-moment correlation length. In the following we do not report the corresponding results. We only mention that they substantially confirm the conclusions drawn from the analysis of the helicity modulus.

The helicity modulus at the BEC transition of the s species is expected to behave as

$$R_s \equiv \Upsilon_s L \approx f(u L^{1/\nu}), \qquad (7)$$

where ν is the correlation-length exponent and the linear scaling field u is a linear combination of T and the model parameters, which vanishes at the critical point. Assuming for simplicity that μ_2 is fixed, at a generic critical point (T_c, μ_{1c}), the scaling field can be written as

$$u(T,\mu_1) \approx a(T - T_c) + b(\mu_1 - \mu_{1c}), \qquad (8)$$

where a and b are nonuniversal coefficients. In particular, we have $u = a(T - T_c)$ if we investigate the transition by varying T keeping μ_1 fixed and $u = b(\mu_1 - \mu_{1c})$ if we vary μ_1 keeping T fixed. The scaling function $f(x)$ is universal, provided coefficients a and b appearing in Eq. (8) are properly defined. However, it depends on the shape and boundary conditions of the system. A straightforward consequence of Eq. (7) is that the curves $R_s(L;\mu_1)$ at fixed L cross each other at the critical point, where their slopes are controlled by the correlation-length exponent ν.

We wish now to verify our conjecture that the critical behavior of the condensing component always belongs to the 3D XY universality class, irrespective of the (normal or superfluid) state of the spectator component. If true, the exponent ν appearing in Eq. (7) equals that of the 3D XY universality class [57] $\nu_{XY} = 0.6717(1)$. Moreover, also the
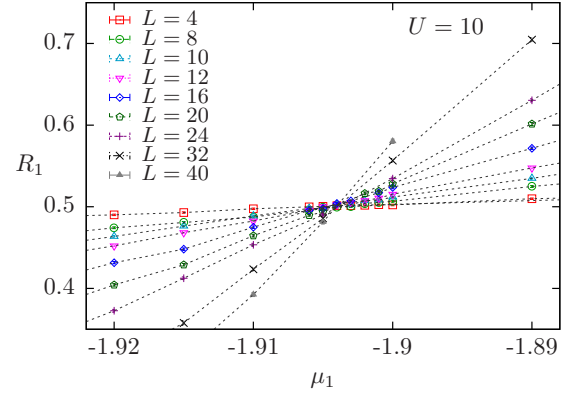

FIG. 6. Helicity-modulus combination R_1 at $T = 1$, $\mu_2 = 0$, and $U = 10$ as a function of μ_1, close to the normal-to-superfluid transition.

scaling function $f(x)$ must be equal to that of the 3D XY universality class apart from a trivial multiplicative rescaling of the argument. In particular, we should find [57] $R^* = f(0) = 0.516(1)$ at the transition.

We should note that an accurate determination of the critical parameters requires us to take into account the corrections to the asymptotic scaling behavior (7). Including the leading corrections we have

$$R_s \approx f(u L^{1/\nu}) + L^{-\omega} g(u L^{1/\nu}), \qquad (9)$$

where $g(x)$ is a scaling function and ω a universal exponent. For the standard 3D XY universality class we know that [57,58] $\omega_{XY} = 0.785(20)$.

B. Finite-size scaling at the transition lines

In the MF approximation, for $\mu_2 = 0$, $U = 10$, and sufficiently small temperature values, the system undergoes three different phase transitions as μ_1 is decreased at fixed T (see Fig. 2). (i) First, starting from large values of μ_1, component 1 undergoes a normal-to-superfluid transition, while component 2 remains in the normal phase. (ii) As μ_1 is further decreased, also component 2 condenses, while component 1 is in the superfluid phase. (iii) Finally, a second normal-to-superfluid transition of component 1 occurs, but in this case the second component is superfluid.

Figures 6–8 show QMC results at $T = 1$ for transition (iii) at $\mu_1 < 0$, up to $L = 40$. The estimates of R_1 show a crossing point at $\mu_{1c} \approx -1.904$ (see Fig. 6), indicating that component 1 undergoes a phase transition, while R_2 increases linearly with L (see Fig. 7), which is the appropriate behavior expected for a gas in the superfluid phase.

In order to check that the critical behavior belongs to the 3D XY universality class, we verify that the data are consistent with Eq. (9), taking the XY values for the critical exponents. In practice, we fit the data to

$$R = R^* + \sum_{i=1}^{m} a_i u^i L^{-i/\nu_{XY}} + L^{-\omega_{XY}} \sum_{j=0}^{n} b_j u^j L^{-j/\nu_{XY}}, \qquad (10)$$

with $u = \mu_1 - \mu_{1c}$. We set $\nu_{XY} = 0.6717$ and $\omega_{XY} = 0.785$, which are the best available estimates of the two exponents for the 3D XY universality class. For our data $u L^{-1/\nu_{XY}}$ is small, so
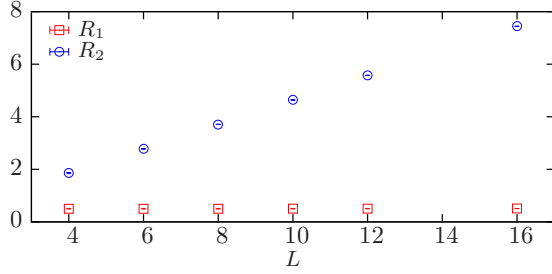
FIG. 7. Plot of $R_s = \Upsilon_s L$ for the two gases at the normal-to-superfluid transition of gas 1, for $T = 1$, $U = 4$, $\mu_2 = 0$, and $\mu_1 = -1.9035$. For $L \to \infty$, R_1 approaches the XY critical value $R^* = 0.516(1)$, while R_2 increases linearly with L as is appropriate for a gas in the superfluid phase.

we have replaced the scaling functions $f(x)$ and $g(x)$ with their expansions (to order m and n, respectively) around $x = 0$. The values of m and n have been chosen by checking the quality of the fit and the stability of the results with respect to the order of the expansions. Around $\mu_1 \approx -1.905$, good fits are obtained by taking $m = 1$ or 2 and $n = 0$. Correspondingly, we estimate $\mu_{1c} = -1.9035(5)$. The quality of this XY-biased fit can be checked by plotting $R_1(L; \mu_1)$ versus $u L^{1/\nu_{XY}}$ with $u = \mu_1 - \mu_{1c}$ (see Fig. 8). We observe a good collapse of the data, confirming the XY nature of the transition.

This FSS analysis confirms the conjecture that the critical behaviors along the normal-to-superfluid transition lines of a single species belong to the 3D XY universality class, even when the other species is in the superfluid phase. Moreover, corrections to scaling appear to decay as $L^{-\omega_{XY}}$, where ω_{XY} is the leading irrelevant exponent for the XY universality class. Therefore, the interactions between the critical and the noncritical component give rise to corrections that are quite suppressed, decaying at least as fast as $L^{-\omega_{XY}}$.

C. Phase diagram for $\mu_2 = 0$ and $U = 4$

For $\mu_2 = 0$ and $U = 4$ we have repeated the FSS analysis of Sec. IV B for other values of the model parameters, with the purpose of determining an approximate phase diagram,
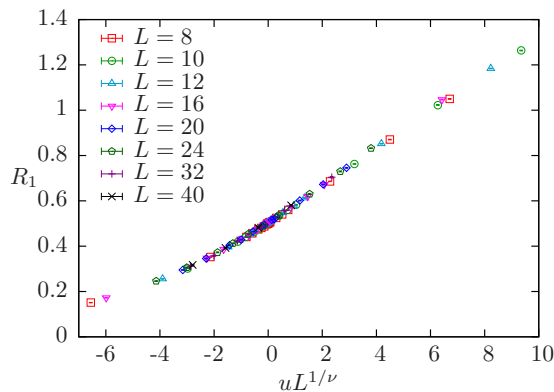

FIG. 8. Helicity modulus combination R_1 (we plot the same data reported in Fig. 6) versus $u L^{1/\nu}$, $u = \mu_1 - \mu_{1c}$, taking ν equal to the XY value $\nu_{XY} = 0.6717$. We use $\mu_{1c} = -1.9035$, obtained by fitting the data to Eq. (10).
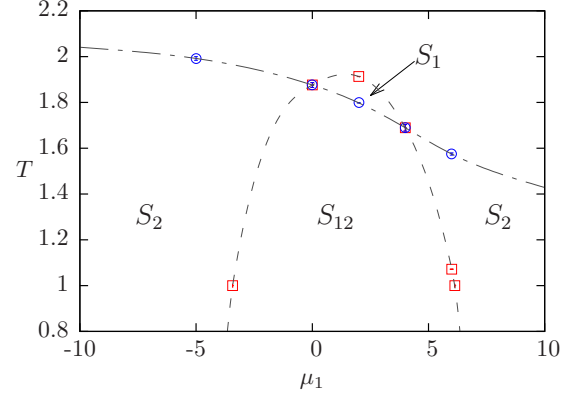

FIG. 9. Phase diagram of the 3D 2BH model (1) in the HC limit, for $\mu_2 = 0$ and $U = 4$, as a function of μ_1 and T. Transitions where component 1 condenses are labeled with squares and those where component 2 condenses with circles. The interpolating lines are only meant to guide the eye. The same phase diagram, computed in the MF approximation, is shown in Fig. 2.

to be compared with that obtained in the MF approximation (see Fig. 2). Our numerical results are in qualitative agreement with the MF predictions, confirming the presence of two MCPs where four transition lines meet (see Fig. 9).

To verify the predicted behavior we have performed simulations at different values of μ_1, $\mu_1 = -5$, 2, and 6, varying the temperature T. In Fig. 10 we show the helicity modulus of the two gases at $\mu_1 = 2$ as a function of $\beta = 1/T$. We observe that R_1 and R_2 cross at two different values of T, indicating the presence of two separate (but close) normal-to-superfluid transitions. If we move down from the high-temperature phase decreasing T, we first observe the condensation of gas 1 at $T_c = 1.9131(4)$ and then that of gas 2 at $T_c = 1.7982(3)$. Two different transitions are also observed at $\mu_1 = 6$. Here, however, the order is reversed. Decreasing the temperature, first gas 2 condenses at $T_c = 1.575(5)$ and then gas 1 condenses at $T_c = 1.072(1)$. At $\mu_1 = -5$ we have observed only one transition, related to component 2. We have also considered a different line in the phase diagram, keeping the temperature fixed $T = 1$ and varying μ_1. In this case we observe two normal-to-superfluid transitions of the
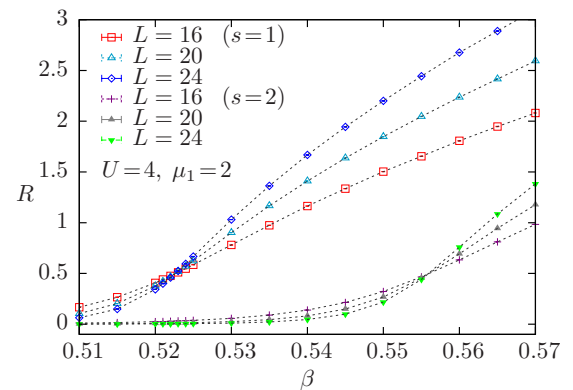

FIG. 10. Estimates of R_1 and R_2 versus $\beta \equiv 1/T$ at $\mu_2 = 0$, $U = 4$, and $\mu_1 = 2$. Two different crossing points are visible, providing evidence for two distinct transitions.
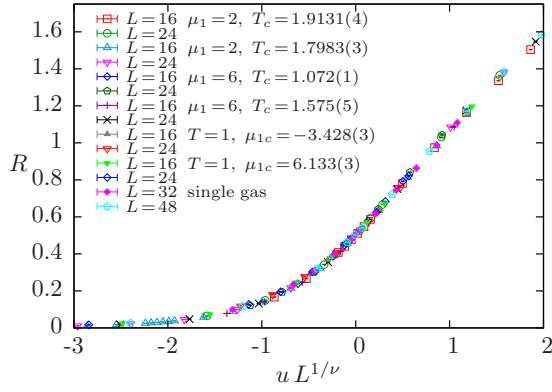
FIG. 11. The FSS plot of the helicity modulus of the condensing species at various normal-to-superfluid transitions for $\mu_2 = 0$ and $U = 4$. The corresponding critical values in the T-μ_1 plane are indicated in the labels. We show data at $\mu_1 = 2$ (at the two transitions considered in Fig. 10), $\mu_1 = 6$ (at the normal-to-superfluid transitions of both gases), and $T = 1$ at the two transitions of gas 1 driven by μ_1. For comparison, we also report results for the BEC transition of the single-species Bose-Hubbard model at $\mu = 0$ and in the HC limit. The data are plotted versus $uL^{1/\nu}$, where $\nu = \nu_{XY} = 0.6717$, $u = a(T - T_c)$ for the transitions at fixed μ_1, and $u = b(\mu_1 - \mu_{1c})$ for those at fixed T [see Eq. (8)]. The constants a or b (they assume different values at each transition) are optimized to obtain the best collapse of the data.

same component, gas 1, at the boundaries of the superfluid phase S_{12}, at $\mu_1 = 6.133(3)$ and $\mu_1 = -3.428(3)$.

Finite-size scaling analyses analogous to those described in Sec. IV B confirm that all transitions belong to the 3D XY universality class. As a further check, in Fig. 11 we show the helicity modulus close to the transitions we have investigated, as a function of $uL^{1/\nu_{XY}}$. By tuning appropriately the constants a or b [cf. Eq. (8)], at each transition (if our data are obtained at fixed $\mu_1 = \mu_{1c}$ we optimize the constant a, while if data are obtained at fixed $T = T_c$ we optimize b) we obtain a perfect collapse of the data, confirming the universality of the scaling function $f(x)$ defined in Eq. (7). We also report the helicity modulus at the BEC transition of a single HC Bose-Hubbard gas. Results fall on top of those obtained for the mixture, confirming the XY nature of the transition.

As already anticipated by the MF computations, the phase diagram reported in Fig. 9 has two MCPs, where four transition lines meet. At each MCP, both gases simultaneously condense. Their locations can be inferred from the numerical results of Ref. [50], where the finite-temperature BEC transitions of the 2BH model for two equal bosonic gases were studied. In particular, when $\mu_1 = \mu_2 = 0$, the two identical gases condense at $T_c = 1.88(1)$ for $U = 4$ and at $T_c = 1.69(1)$ for $U = -4$. Using the particle-hole relation (2), the latter transition implies an analogous transition at $\mu_1 = 4$, $\mu_2 = 0$, $U = 4$, and $T_c = 1.69(1)$. Clearly, the two transitions at $U = 4$, $\mu_1 = 0$, $\mu_2 = 0$, $T_{MC} = 1.88(1)$ and $U = 4$, $\mu_1 = 4$, $\mu_2 = 0$, $T_{MC} = 1.69(1)$ must correspond to the MCPs of the phase diagram reported in Fig. 9, since they are characterized by the simultaneous BEC of both gases.

As shown in Ref. [50], the critical behavior of the transition of two equal HC bosonic gases with on-site interspecies density-density interaction is controlled by a decoupled XY

FP. However, in this case the competition of the two U(1) order parameters leads to unusual slowly decaying scaling corrections. Indeed, the interspecies density-density interaction gives rise to scaling corrections that decay very slowly, as $\xi^{-0.022}$, where ξ is the diverging length scale at the transition. Such scaling corrections are not present in standard transitions belonging to the XY universality class, where they decay as $\xi^{-\omega_{XY}}$ with $\omega_{XY} \approx 0.78$.

V. MULTICRITICAL BEHAVIORS

The competition of distinct types of order gives generally rise to multicritical phenomena. More specifically, a MCP is observed at the intersection of two critical lines characterized by different order parameters. Multicritical behaviors occur in several physical contexts: in anisotropic antiferromagnets, high-T_c superconductors, multicomponent polymer solutions, disordered systems, etc. (see, e.g., Refs. [62–77]).

The phase diagrams obtained in the previous sections show various MCPs (see, e.g., Figs. 2 and 5 in Sec. III and Fig. 9 in Sec. IV, where BEC transition lines meet). At the MCP, the competition of the two order parameters gives rise to peculiar critical properties. Their scaling behaviors are controlled by the stable fixed point (FP) of the RG flow, which can be studied by field-theoretic approaches based on the appropriate multicritical Landau-Ginzburg-Wilson (LGW) Φ^4 theory describing two interacting complex order-parameter fields.

A. Multicritical U(1)⊕ U(1) LGW Φ^4 theory

The LGW theory describing the competition of the two different U(1) order parameters is obtained by constructing the most general Φ^4 theory of two complex fields $\varphi_s(\boldsymbol{x})$, which is invariant under independent U(1) transformations acting on each of them. Its Hamiltonian is

$$\mathcal{H}_{\text{LGW}} = \int d^3x \left[\sum_{s,\mu} |\partial_\mu \varphi_s|^2 + \sum_s r_s |\varphi_s|^2 \right.$$
$$\left. + \frac{1}{24} \sum_s v_s |\varphi_s|^4 + \frac{1}{4} u |\varphi_1|^2 |\varphi_2|^2 \right], \quad (11)$$

with two quadratic parameters r_1 and r_2 and three quartic parameters v_1, v_2, and u. A multicritical behavior is obtained by tuning the quadratic parameters r_1 and r_2 simultaneously to their critical values, keeping the quartic parameters fixed. Note that the theory is well defined (the quartic potential is bounded from below) for $v_1 > 0$, $v_2 > 0$, and $u > -\frac{1}{3}\sqrt{v_1 v_2}$.

Mean-field calculations show that the U(1)⊕ U(1) LGW theory (11) leads to two different phase diagrams [64,65,74] (see Fig. 12), depending on the sign of $\Delta \equiv v_1 v_2 - 9u^2$. If $\Delta > 0$, four critical lines meet at the MCP (tetracritical behavior), as in the left panel of Fig. 12, while if $\Delta < 0$, two critical lines and one first-order line (bicritical behavior) meet at the MCP (see the right panel of Fig. 12). Note that, in the HC limit, the 2BH model should correspond to the LGW theory with $\Delta > 0$, because of the correspondence $V_s \sim v_s$ and $U \sim u$. Therefore, we expect a tetracritical behavior. A bicritical behavior is expected instead in the opposite limit $V_s \lesssim U$. The MF results presented in Sec. III are completely consistent with this prediction.
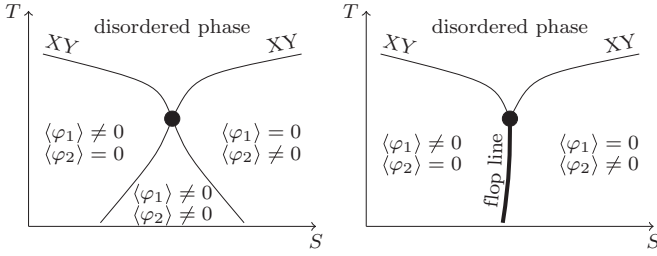
FIG. 12. Different phase diagrams for models with two different interacting U(1) order parameters. In the left panel the MCP is observed at the point where four transition lines meet (tetracritical point); all transitions are continuous. In the right panel two continuous transitions (thin lines) and one first-order transition (thick line) meet at the MCP (bicritical point).

B. Multicritical scaling

In the LGW theory the transition lines appearing in Fig. 12 are obtained by tuning one of the two quadratic parameters r_1 and r_2 to its critical value. Multicritical behaviors arise when both of them are tuned to criticality. Therefore, generic multicritical behaviors are associated with two relevant scaling fields w_1 and w_2 (analytic functions of the model parameters such that $w_1 = w_2 = 0$ at the MCP) with positive RG dimensions y_1 and y_2. For example, in the case of the 2BH model (1) w_1 and w_2 may be taken as linear combinations of the temperature and the chemical potentials of the two gases. In the absence of external fields, the singular part of the free-energy density is expected to obey the scaling law

$$F_{\text{sing}}(w_1, w_2, w_3, \ldots) = b^{-d} \mathcal{F}(b^{y_1} w_1, b^{y_2} w_2, b^{y_3} w_3, \ldots), \quad (12)$$

where b is an arbitrary *blocking* variable. Here we consider additional irrelevant scaling fields w_i, $i \geqslant 3$ with RG dimensions $y_i < 0$, that give rise to scaling corrections at the critical point. Neglecting their contribution and appropriately fixing the arbitrary variable b as $b = |w_1|^{-1/y_1}$, we obtain the asymptotic scaling expression

$$F_{\text{sing}} \approx |w_1|^{d/y_1} f_\pm(w_2 |w_1|^{-y_2/y_1}), \quad (13)$$

where $f_\pm$ are universal scaling functions, which depend on the sign of w_1: $f_+(x)$ should be considered for $w_1 > 0$ and $f_-(x)$ in the opposite case. Close to the MCP, all transition lines correspond to constant values of the product $w_2 |w_1|^{-y_2/y_1}$.

Within the LGW theory, a standard multicritical behavior can only be observed if there exists a stable FP for the corresponding RG flow and the system is in its attraction domain. In the opposite case, the flow generically runs to infinity and the transition is discontinuous. Note that this can also occur if a stable FP exists, but the system is outside its attraction domain.

We should note that the unstable FPs of the theory also can be associated with more complicated multicritical behaviors. In this case one should perform additional tunings of the parameters and correspondingly introduce additional relevant scaling fields. For example, consider a FP that is unstable with respect to one of the RG quartic perturbations, i.e., such that the flow ends at the FP only if one performs one additional tuning of the initial parameters. This means that there is an additional relevant scaling field. Equation (12) still holds, but

now $y_3 > 0$. Therefore, the contribution of w_3 can no longer be neglected approaching the critical point. From a more phenomenological point of view, this higher-order multicritical behavior can be observed by varying three model parameters. In the corresponding parameter space, one has surfaces of standard critical transitions. These surfaces intersect along lines that correspond to standard multicritical behavior. The transition may be continuous, controlled by the stable FP, or of first order, if the RG flow goes to infinity. The higher-order multicritical behavior is observed at the intersection of the multicritical lines. Of course, such points are quite difficult to observe in practice.

C. Perturbative field-theoretic expansion

The critical behavior at a continuous transition is controlled by the FPs of the RG flow, which are determined by the common zeros of the β functions associated with the parameters appearing in the quartic potential. The presence of a stable FP controls the universal features of the critical behavior if the transition is continuous. If no stable FP exists, the generic transition is expected to be of first order.

The β functions of the theory can be computed using perturbation theory. In the calculation one should be careful to tune r_1 and r_2 to their critical value to obtain the critical theory. This requirement is automatically satisfied if one considers the ϵ expansion, which is based on dimensional regularization around four dimensions [78]. Indeed, in this regularization scheme, one considers directly the massless critical theory. The same is true in the related 3D scheme of Ref. [79], the so-called minimal subtraction ($\overline{\text{MS}}$) scheme without ϵ expansion. Here one also considers the $\overline{\text{MS}}$ perturbative series, but does not expand in powers of ϵ, setting $\epsilon = 1$.

The Hamiltonian fields and parameters are renormalized [80] by setting $\varphi_s = Z_s^{1/2} \varphi_{sr}$, $v_s = A_d \mu^\epsilon Z_{v_s}(v_{sr}, u_r)$, and $u = A_d \mu^\epsilon Z_u(v_{sr}, u_r)$, where v_{sr} and u_r are the $\overline{\text{MS}}$ renormalized quartic couplings. The five renormalization functions Z_s and $Z_{v_s, u}$ are normalized so that $Z_s \approx 1$, $Z_{v_s} \approx v_s$, and $Z_u \approx u$ at tree level. Here A_d is a d-dependent constant given by $A_d \equiv 2^{d-1} \pi^{d/2} \Gamma(d/2)$. The $\overline{\text{MS}}$ β functions are obtained by differentiating the renormalized couplings with respect to the scale μ, keeping the bare couplings v_1, v_2, and u fixed. The two-loop β functions associated with the quartic couplings are

$$\beta_{v_1} = -\epsilon v_{1r} + \tfrac{5}{3} v_{1r}^2 + 3 u_r^2 - \tfrac{5}{3} v_{1r}^3 - \tfrac{5}{2} v_{1r} u_r^2 - 6 u_r^3,$$

$$\beta_{v_2} = -\epsilon v_{2r} + \tfrac{5}{3} v_{2r}^2 + 3 u_r^2 - \tfrac{5}{3} v_{2r}^3 - \tfrac{5}{2} v_{2r} u_r^2 - 6 u_r^3,$$

$$\beta_u = -\epsilon u_r + 2 u_r^2 + \tfrac{2}{3} v_{1r} u_r + \tfrac{2}{3} v_{2r} u_r - \tfrac{5}{2} u_r^3$$
$$\quad - 2 v_{1r} u_r^2 - 2 v_{2r} u_r^2 - \tfrac{5}{18} v_{1r}^2 u_r - \tfrac{5}{18} v_{2r}^2 u_r. \quad (14)$$

The complete five-loop series are reported in the Appendix.

The zeros of the β functions provide the location of the FPs of the RG flow. Their stability is controlled by the matrix $\Omega_{i,j} = \partial \beta_i / \partial g_j$ [the indices correspond to the three quartic couplings $\mathbf{g} \equiv (v_1, v_2, u)$] evaluated at the given FP. The FP is stable if all eigenvalues ω_i of the stability matrix have a positive real part.

D. Renormalization-group flow and FPs close to four dimensions

We first determine the FPs and their stability properties close to four dimensions, using the first few terms of the standard ϵ expansion [81]. We find six different FPs, of which the only stable one is located at

$$v_{1r} = v_{2r} = \frac{1}{2}\epsilon + \frac{7}{16}\epsilon^2 + O(\epsilon^3),$$
$$u_r = \frac{1}{6}\epsilon - \frac{1}{48}\epsilon^2 + O(\epsilon^3). \qquad (15)$$

In the general $O(n_1) \oplus O(n_2)$ model this FP is named biconical FP [64,65] and it generally satisfies $v_{1r} \neq v_{2r}$. In the U(1)$\oplus$ U(1) case, however, $v_{1r} = v_{2r}$ and therefore this FP also appears in the theory with $v_1 = v_2$ and $r_1 = r_2$,

$$\mathcal{H}_{\text{LGW}} = \int d^3x \left[\sum_{s,\mu} |\partial_\mu \varphi_s|^2 + r \sum_s |\varphi_s|^2 \right.$$
$$\left. + \frac{v}{24} \sum_s |\varphi_s|^4 + \frac{u}{4} |\varphi_1|^2 |\varphi_2|^2 \right], \qquad (16)$$

which is symmetric under the larger symmetry group $\mathbb{Z}_{2,e} \otimes$ [U(1) $\oplus$ U(1)]. Note that this FP is degenerate with the O(4) FP at leading order in ϵ. As a consequence, n-loop calculations at this FP provide results to $O(\epsilon^{n-1})$ only. Thus, the available five-loop series reported in the Appendix allow us to determine the location of the FP only to order ϵ^4. For the same reason the smallest eigenvalue of the stability matrix is of order ϵ^2: $\omega_1 \approx \epsilon^2/6$.

The U(1)$\oplus$ U(1) LGW theory reduces itself to the O(4)-symmetric Φ^4 theory when $r_1 = r_2$ and $v_1 = v_2 = 3u$. Correspondingly, the RG flow has an O(4)-symmetric FP at

$$v_{1r} = v_{2r} = 3u_r = \frac{1}{2}\epsilon + \frac{13}{48}\epsilon^2 + O(\epsilon^3). \qquad (17)$$

This FP is unstable in the full theory (11), since one eigenvalue of the stability matrix is negative, $\omega_1 \approx -\epsilon^2/6$. Therefore, it corresponds to a higher-order multicritical behavior with three relevant scaling fields, of RG scaling dimensions $y_1 \approx 2 - \epsilon/2$, $y_2 \approx 2 - \epsilon/6$, and $y_3 \approx \epsilon^2/6$.

The LGW theory decouples into two identical U(1) Φ^4 theories when $u = 0$. We can therefore identify a decoupled FP (DFP) with $u_r = 0$. At the DFP, the two U(1) order parameters are decoupled, with a critical behavior belonging to the XY universality class. The DFP is located at

$$v_{1r} = v_{2r} = \frac{3}{5}\epsilon + \frac{9}{25}\epsilon^2 + O(\epsilon^3), \quad u_r = 0. \qquad (18)$$

The DFP is stable within each U(1) theory. Therefore, its stability properties in model (11) depend only on the RG dimension y_u of the coupling u associated with the quartic term $|\varphi_1|^2 |\varphi_2|^2$ that couples the two fields. The RG dimension y_u can be evaluated using general scaling arguments [66,69,70,82]. At the DFP, the operator $|\varphi_1|^2 |\varphi_2|^2$ scales as the product of two energylike operators of the d-dimensional XY universality class. Therefore, the RG dimension y_u is given by

$$y_u = \frac{2}{\nu_{XY}} - d. \qquad (19)$$

Using $\nu_{XY} \approx 1/2 + \epsilon/10$, we obtain $y_u \approx \epsilon/5 > 0$. Therefore, the DFP is unstable close to four dimensions.

The other three FPs also have $u_r = 0$. Their stability matrix has two or three negative eigenvalues and hence they can only be observed by tuning four or five different system parameters. They are of little relevance for interacting Bose gases.

The above calculations can be straightforwardly extended to $O(\epsilon^5)$ [$O(\epsilon^4)$ in the case of the stable FP] using the complete series reported in the Appendix. However, methods based on the ϵ expansion allow us to find only those 3D FPs that can be related, by analytic continuation, to those present close to four dimensions. However, new FPs may emerge in three dimensions, which cannot be detected by the ϵ expansion, because they do not have a 4D counterpart. This means that the ϵ expansion may not provide the correct description of the 3D RG flow. For example, this occurs for the Ginzburg-Landau model, in which a complex scalar field is coupled to a gauge field, which is appropriate to describe superconductors and the nematic–smectic-A transition in liquid crystals [83]. Although ϵ-expansion calculations do not find a stable FP [83]—therefore, they predict a first-order transition—numerical analyses show that these systems can also undergo continuous transitions in three dimensions (see, e.g., Refs. [84,85]). This implies the presence of a stable FP in the 3D Ginzburg-Landau theory, in agreement with experiments in liquid crystals [86]. Other examples are provided by the O(2)$\otimes$ O(N) LGW Φ^4 theories describing frustrated spin models with noncollinear order [87,88], the ^{3}He superfluid transition from the normal to the planar phase [89], etc. Therefore, a more conclusive analysis of the RG flow in three dimensions requires a direct 3D study.

E. Fixed points in three dimensions

We now extend the analysis to the 3D case. Since the ϵ expansion suggests that the relevant FPs belong to the plane $v_{1r} = v_{2r}$, we first consider the 3D FPs that appear in the LGW theory (16) and discuss their stability in the multicritical theory in which the exchange symmetry is broken.

The analysis of the FPs for the model (16) is reported in Ref. [50]. Two stable FPs are identified: the DFP and a second FP, named asymmetric FP (AFP). The DFP controls the transitions at which two identical gases condense simultaneously. The AFP instead is the relevant FP for transitions at which only one gas undergoes BEC, breaking the exchange symmetry of the model (16).

Let us now discuss the stability of these two FPs within the multicritical theory (11), starting with the DFP. For $u = 0$ the model corresponds to two noninteracting U(1) systems. We thus obtain for the RG dimensions of the quadratic operators $y_1 = y_2 = 1/\nu_{XY} = 1.4888(3)$. The two quartic perturbations that are present for $u = 0$ can be identified with the quartic perturbation of the standard U(1) theory, so $y_{v_1} = y_{v_2} = -\omega_{XY} = -0.785(20)$. The RG dimension of the perturbation coupling the two XY models can be computed as in the 4D case, using Eq. (19) and $\nu_{XY} = 0.6717(1)$ [57]. We obtain

$$y_u = \frac{2}{\nu_{XY}} - 3 = -0.0225(4), \qquad (20)$$

which is also negative, confirming the stability of the DFP in three dimensions, at variance with the behavior close to four dimensions. Since $u = 0$, we have $\Delta = v_1 v_2 - 9u^2 > 0$.

Thus, the DFP should be relevant for systems that have a tetracritical MCP (see Fig. 12). The asymptotic decoupling of the critical modes allows us to simplify Eq. (12). Neglecting scaling corrections, i.e., setting $w_i = 0$ for $i \geqslant 3$, we can simply rewrite

$$F_{\text{sing}}(w_1, w_2) \approx b^{-d} \mathcal{F}_{XY}(b^{y_1} w_1) + b^{-d} \mathcal{F}_{XY}(b^{y_1} w_2)$$
$$\approx a_{\pm}^{(1)} |w_1|^{3\nu_{XY}} + a_{\pm}^{(2)} |w_2|^{3\nu_{XY}}, \quad (21)$$

where $a_{\pm}^{(a)}$ are constants (related the signs of w_i). By appropriately choosing w_1 and w_2, we can additionally set $a_+^{(1)} = a_+^{(2)} = 1$ so that $a_-^{(1)} = a_-^{(2)}$. The scaling fields are defined by the requirement that the transition lines correspond to $w_1 = 0$ or $w_2 = 0$. Note, however, that the approach to the asymptotic decoupled scaling behavior (21) is characterized by very slowly decaying corrections, due to the small value of RG dimension y_u of the leading irrelevant RG perturbation. As already discussed in Ref. [50], this may make the observation of the asymptotic behavior (21) quite difficult in experiments and numerical studies.

The second stable FP of the reduced theory (16) is the AFP that controls the critical behavior when only one of two bosonic species condenses [50]. It also appears in the O(2)⊗O(2) LGW theory describing the critical modes of some frustrated spin models with noncollinear order [87,90,91]. Within the multicritical theory (11), the AFP should describe bicritical points (right panel of Fig. 12), essentially because it is associated with the BEC of only one species. The RG dimensions of the two relevant perturbations at the AFP correspond to the dimensions of the quadratic operators. The RG dimension y_1 is obtained from the relation $y_1 = 1/\nu$, where ν is the correlation-length exponent of the LGW theory (16). The analysis of the perturbative expansions within two different renormalization schemes [50,87] (the so-called $d = 3$ massive zero-momentum and $\overline{\text{MS}}$ schemes) gives $\nu = 0.57(3)$ and $\nu = 0.65(6)$, respectively, so $y_1 \approx 1.7$. The RG dimension y_2 can be derived from the results reported in Ref. [73] for the quadratic perturbations to the FPs of the O(2)⊗ O(2) theory. We obtain $y_2 = 1.34(15)$ and $y_2 = 1.25(4)$ in the two different perturbative schemes. The stability properties of the AFP within the multicritical theory (11) depend also on the RG dimension y_{v_d} of the quartic coupling $v_d \sim v_1 - v_2$ associated with the operator $P_d = |\varphi_1|^4 - |\varphi_2|^4$ breaking the exchange symmetry. The RG dimension y_{v_d} can be computed by a perturbative analysis in the $\overline{\text{MS}}$ scheme without ϵ expansion. We obtain the estimate $y_{v_d} = -0.6(1)$, where the error takes into account how the estimate changes as the FP position varies within one error bar (we use the FP estimates of Ref. [87]) and the dependence on the resummation parameters. Since $y_{v_d} < 0$, the quartic perturbation P_d is irrelevant and therefore the AFP is stable in the multicritical theory.

It is worth mentioning that the AFP is not connected with the stable biconical FP found close to four dimensions. Indeed, they describe different symmetry-breaking patterns. The stable FP close to four dimensions corresponds to a tetracritical MCP, in contrast with the AFP, which gives rise to a bicritical behavior. Apparently, the biconical FP disappears when approaching three dimensions, while the AFP, which is absent close to four dimensions, appears only close to three dimensions [87].

It is also interesting to discuss the O(4) FP, which is already unstable in the reduced theory (16). A complete analysis shows that there are three different relevant scaling fields at the O(4) FP in the full theory (11). Summarizing, the RG dimensions of the relevant scaling fields are $y_1 = 1.333(4)$ associated with the scalar quadratic perturbation at the O(4) FP [obtained using $\nu = 1/y_1 = 0.750(2)$ [92,93]], $y_2 = 1.813(6)$ associated with the spin-2 quadratic perturbation [71], and $y_3 = 0.125(5)$ associated with the spin-4 quartic perturbation [71,92].

The analysis we have presented considers only the FPs with $v_{1r} = v_{2r}$. *A priori* other FPs may be present with $v_{1r} \neq v_{2r}$. As we will see in the next section, the analysis of the general RG flow does not find any evidence of additional stable FPs.

F. Three-dimensional RG flow

In this section we study the RG flow. In particular, we determine the RG trajectories starting from the Gaussian FP, where the quartic couplings vanish. This study allows us to determine the stable FPs and their attraction domain in the space of the Hamiltonian (bare) quartic parameters. We use here the $\overline{\text{MS}}$ scheme without ϵ expansion [79], which provides a genuine 3D critical scheme.

The RG trajectories are obtained by solving the differential equations

$$-\lambda \frac{du_r}{d\lambda} = \beta_u[u_r(\lambda), v_{sr}(\lambda)],$$
$$-\lambda \frac{dv_{sr}}{d\lambda} = \beta_{v_s}[u_r(\lambda), v_{sr}(\lambda)], \quad (22)$$

where $s = 1, 2$, $\lambda \in [0, \infty)$, with the initial conditions

$$u_r(0) = v_{s\,r}(0) = 0,$$
$$\left.\frac{du_r}{d\lambda}\right|_{\lambda=0} = u, \quad \left.\frac{dv_{sr}}{d\lambda}\right|_{\lambda=0} = v_s. \quad (23)$$

Note that the trajectories do not depend on the Hamiltonian parameters individually, but only through their dimensionless ratios. For this purpose, we rescale $\lambda \to \lambda/\sqrt{v_1 v_2}$ so that the initial conditions become $R_u = u/\sqrt{v_1 v_2}$ for $du_r/d\lambda$, and $R_v = \sqrt{v_1/v_2}$ and $1/R_v$ for the derivatives of $dv_{1r}/d\lambda$ and $dv_{2r}/d\lambda$, respectively. Note that the LGW theory (11) is stable for $R_u > -1/3$. Since $\Delta = v_1 v_2(1 - 9R_u^2)$, one expects tetracritical or bicritical behavior if $-1/3 < R_u < 1/3$ and $R_u > 1/3$, respectively. Moreover, the symmetry of the model under $v_1 \to v_2$ and $v_2 \to v_1$ allows us to restrict the analysis to $0 \leqslant R_v \leqslant 1$. To obtain meaningful results, the perturbative series are resummed by employing the Padé-Borel technique (see, e.g., Refs. [58,80]).

Typical results are shown in Fig. 13, where we report a projection of the trajectories in the (v_{1r}, u_r) plane for $R_v = 1/2$ (results for other values of R_v are qualitatively analogous). For R_u slightly larger than $-1/3$ (see the behavior for $R_u = -0.20$ in the figure), it is not possible to follow the flow beyond a certain value of λ, since the Borel transform becomes singular on the positive real axis. These trajectories clearly correspond to systems that undergo discontinuous transitions. If we further increase R_u, we observe that trajectories flow to the DFP, which is the stable FP relevant for small values of u. If R_u is increased again, the relevant FP changes and the trajectories end up at the
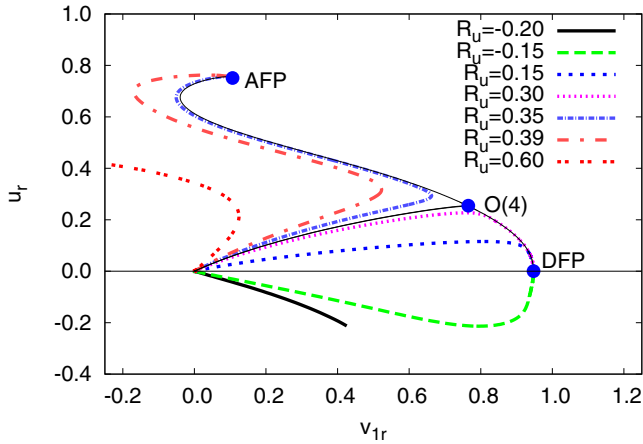
FIG. 13. The RG flow as a function of v_{1r} and u_r, for $R_v = 1/2$ and several values of R_u, in the $\overline{\text{MS}}$ scheme without ϵ expansion. We also report the positions of the O(4) unstable fixed point, of the DFP, and of the AFP. Thin solid lines correspond to the separatrices of the RG flow, connecting the different FPs.

AFP. If R_u is further increased, trajectories run into the non-Borel summable region $v_{1r} < 0$ and $v_{2r} < 0$ (see the behavior for $R_u = 0.60$ in the figure). It is interesting to observe that the range of values of R_u corresponding to trajectories flowing to the AFP is quite small. For the approximant shown in the figure, we should have $0.33 \lesssim R_u \lesssim 0.40$. For any $R_u \gtrsim 0.40$ the trajectories flow to infinity. This suggests that most of the bicritical MCPs undergo first-order transitions. Note that the numerical analysis does not provide any evidence of additional FPs. Apparently, all relevant FPs belong to the symmetric model with $v_1 = v_2$.

G. Implications for the Bose-Hubbard model of two lattice bosonic gases

The above RG analysis applies to generic mixtures of bosonic gases with short-range density-density interspecies interactions, which have global U(1)⊕ U(1) symmetry, and, in particular to the 2BH model (1). In the hard-core limit of both gases, the MCPs are predicted to be tetracritical (see left panel of Fig. 12), consistently with the numerical results shown in Fig. 9. The multicritical behavior is controlled by the DFP, with slowly decaying scaling corrections. At the MCP there is an asymptotic decoupling of the critical modes associated with the two components [see e.g., Eq. (21) for the singular part of the free energy].

On the other hand, 2BH models in the soft-core regime $V_s \lesssim U$ correspond to LGW Φ^4 models with $\Delta < 0$. Thus, they should present bicritical points (see the right panel of Fig. 12), consistently with the mean-field analysis presented in Fig. 5. In this region continuous multicritical behaviors are controlled by the other stable AFP, which leads to the nontrivial scaling behavior (13) describing entangled BEC critical modes.

VI. CONCLUSION

In this paper we studied the critical and multicritical behaviors that can be observed in 3D mixtures of bosonic gases interacting by short-range density-density interactions.

These systems have a global U(1)⊕ U(1) symmetry, related to independent U(1) transformations acting on each species. As a representative of this class of systems, we considered the 3D Bose-Hubbard model for two lattice bosonic gases coupled by an on-site interspecies density-density interaction, whose Hamiltonian is given in Eq. (1). However, the qualitative features of the finite-temperature phase diagram and the results for the universality classes associated with the critical and multicritical behaviors apply to generic bosonic mixtures.

The generic features of the phase diagram of the 2BH model have been determined in the MF approximation and additionally confirmed by QMC simulations. The qualitative behavior depends on the model parameters, such as the chemical potentials and the on-site interspecies and intraspecies couplings. By varying them, one can observe several transition lines, along which one of the two species undergoes a normal-to-superfluid transition, and different types of multicritical behavior.

The transition lines separating the different phases generally correspond to the BEC condensation of one of the two species. We showed that, independently of whether the other species is in the normal or superfluid phase, the critical behavior of the condensing species belongs to the 3D XY universality class, characterized by the breaking of a global U(1) symmetry and short-range effective interactions, which is the same universality class associated with the BEC of a single bosonic gas. Therefore, the critical modes of the condensing gas effectively decouple from those of the other species, independently of whether the latter is in the normal or superfluid phase.

The phase diagram of mixtures of bosonic gases also presents particular points where some transition lines meet. At these points multicritical behaviors develop, due to the competition of the U(1) order parameters related to the two bosonic gases. We investigated them using a field-theoretic approach based on the effective LGW Φ^4 theory for two complex scalar fields with global U(1)⊕ U(1) symmetry. The possible universality classes that describe the multicritical behaviors are associated with the stable FPs of the RG flow. They can be determined by studying the RG trajectories in the critical theory, starting from the unstable Gaussian FP in the quartic-parameter space. For this purpose, we considered the so-called $\overline{\text{MS}}$ scheme without ϵ expansion [79]. We started from the five-loop $\overline{\text{MS}}$ β functions, resummed them using the Padé-Borel technique, and solved the flow equations. We found two stable FPs, which also belong to the Φ^4 theory (16), which has an additional $\mathbb{Z}_2$ symmetry related to the exchange of the two order parameters. This more symmetric model has already been discussed in the context of the critical behavior of a mixture of two identical gases [50]. If the system has a tetracritical continuous transition (see Fig. 12), the critical behavior is controlled by a decoupled FP. Each component shows an XY critical behavior—correspondingly, the RG dimensions of the two relevant operators are $y_1 = y_2 \approx 1.49$— but with very slowly decaying scaling corrections (they decay as $\xi^{-0.022}$, where ξ is the correlation length) due to interspecies coupling. If instead the system undergoes a bicritical continuous transition, the critical behavior is associated with a different asymmetric FP, with $y_1 \approx 1.7$ and $y_2 \approx 1.3$.

The above results apply to the MCPs that can be observed in generic mixtures of bosonic gases with short-range density-density interspecies interactions, which realize systems with global U(1)⊕ U(1) symmetry. In particular, they apply to the MCPs of mixtures of lattice bosonic gases described by the Bose-Hubbard model (1). The RG analysis of the U(1)⊕ U(1) LGW Φ^4 theory predicts tetracritical and bicritical points in the hard-core $V_s \gtrsim U$ and soft-core $V_s \lesssim U$ regimes, respectively, associated with different universality classes, controlled by the stable decoupled and asymmetric FPs, respectively.

Recent experiments on atomic gas mixtures [1–22], using either two different atomic species or the same atomic species in two different states, have already obtained several interesting results on the properties of the low-temperature condensed phase and on the interplay of the different condensates. They have also demonstrated the possibility of a robust control of the model parameters, which may allow the observation of the different phases, such as those found in the present study, and the determination of the nature of the critical and multicritical behaviors. Our results should provide a complete characterization of the possible BEC patterns and of the critical behaviors that these systems may develop along their transition lines. Our findings may be also relevant for possible applications of degenerate bosonic mixtures in optical lattices as analog quantum simulation devices [94].

Most cold-atom experiments have been performed in inhomogeneous conditions, due to the presence of space-dependent trapping forces, which effectively confine the atomic gas within a limited space region [51]. The trapping potential is effectively coupled to the particle density, which may be taken into account by adding a further Hamiltonian term to the 2BH Hamiltonian (1), i.e., $H_{\text{trap}} = \sum_{s\boldsymbol{x}} V_s(\boldsymbol{x}) n_{s\boldsymbol{x}}$, where V_s is the space-dependent potential associated with the external force. The inhomogeneity arising from the trapping potential introduces an additional length scale ℓ_t into the problem, which drastically changes the general features of the behavior at the phase transitions. Experimental data for inhomogeneous trapped cold-atom systems are usually analyzed using the local-density approximation (see, e.g., Ref. [51]). However, this approach fails to describe the emergence of large-scale correlations [40,54]. This problem may be overcome experimentally by using (almost) flat traps, giving rise to a finite space region where the system is effectively homogenous [95]. Otherwise, one may infer the critical behavior by studying the scaling behavior with respect to the trap size ℓ_t, which is expected to be universal and controlled by the critical exponents of the universality class of the corresponding homogenous system, in the large trap-size limit [38,54,55,96].

APPENDIX : FIVE-LOOP SERIES OF THE U(1)⊕ U(1) LGW THEORY

We report here the five-loop perturbative series of the β functions used in Sec. V F to analyze the RG flow of the U(1)⊕ U(1) LGW Φ^4 theory. We consider the perturbative expansions obtained in $4 - \epsilon$ dimensions, using the dimensional regularization and in the modified $\overline{\text{MS}}$ scheme. They were computed in Ref. [71] for general O(n_1)⊕ O(n_2) theories, but they were not reported there. Apart from the first few orders, coefficients are reported with a 10^{-6} numerical precision, although they are computed in terms of fractions and ζ functions (the exact series are available on request). To simplify the formulas, the renormalized couplings are named v_1, v_2, and u instead of v_{1r}, v_{2r}, and u_r. The five-loop β functions read

$$
\begin{aligned}
\beta_{v_1}(v_1,v_2,u) = {} & -\epsilon v_1 + \tfrac{5}{3}v_1^2 + 3u^2 - \tfrac{5}{3}v_1^3 - \tfrac{5}{2}v_1 u^2 - 6u^3 + 14.381 u^4 + 36.1747 v_1 u^3 + 8 v_2 u^3 \\
& + 2.3125 v_1^2 u^2 + 0.125 v_2^2 u^2 - 1.08333 v_1 v_2 u^2 + 4.99347 v_1^4 - 120.062 u^5 - 164.419 v_1 u^4 - 91.2808 v_2 u^4 \\
& - 165.154 v_1^2 u^3 - 10.9914 v_2^2 u^3 - 18.2281 v_1 v_2 u^3 - 5.32929 v_1^3 u^2 - 0.489598 v_2^3 u^2 - 0.144409 v_1 v_2^2 u^2 \\
& + 0.969685 v_1^2 v_2 u^2 - 21.9072 v_1^5 + 1090.1 u^6 + 1633.45 v_1 u^5 + 947.957 v_2 u^5 + 1140.29 v_1^2 u^4 \\
& + 257.256 v_2^2 u^4 + 608.06 v_1 v_2 u^4 + 950.994 v_1^3 u^3 + 37.2454 v_2^3 u^3 + 32.3079 v_1 v_2^2 u^3 + 35.291 v_1^2 v_2 u^3 \\
& + 6.68047 v_1^4 u^2 + 1.27762 v_2^4 u^2 - 0.142137 v_1 v_2^3 u^2 + 1.6941 v_1^2 v_2^2 u^2 + 2.20787 v_1^3 v_2 u^2 + 120.141 v_1^6, \quad \text{(A1)}
\end{aligned}
$$

$$
\beta_{v_2}(v_1,v_2,u) = \beta_{v_1}(v_2,v_1,u), \tag{A2}
$$

$$
\begin{aligned}
\beta_u(v_1,v_2,u) = {} & -\epsilon u + 2u^2 + \tfrac{2}{3}v_1 u + \tfrac{2}{3}v_2 u - \tfrac{5}{2}u^3 - 2v_1 u^2 - 2v_2 u^2 - \tfrac{5}{18}v_1^2 u - \tfrac{5}{18}v_2^2 u \\
& + 11.7312 u^4 + 11.3082 v_1 u^3 + 11.3082 v_2 u^3 + 3.50134 v_1^2 u^2 + 3.50134 v_2^2 u^2 + 1.11111 v_1 v_2 u^2 + 0.652778 v_1^3 u \\
& + 0.652778 v_2^3 u - 85.8801 u^5 - 87.0641 v_1 u^4 - 87.0641 v_2 u^4 - 38.5894 v_1^2 u^3 - 38.5894 v_2^2 u^3 - 32.9072 v_1 v_2 u^3 \\
& - 12.3167 v_1^3 u^2 - 12.3167 v_2^3 u^2 - 2.06356 v_1 v_2^2 u^2 - 2.06356 v_1^2 v_2 u^2 - 1.99192 v_1^4 u - 1.99192 v_2^4 u + 711.585 u^6 \\
& + 896.552 v_1 u^5 + 896.552 v_2 u^5 + 455.484 v_1^2 u^4 + 455.484 v_2^2 u^4 + 507.235 v_1 v_2 u^4 + 176.847 v_1^3 u^3 + 176.847 v_2^3 u^3 \\
& + 95.0588 v_1 v_2^2 u^3 + 95.0588 v_1^2 v_2 u^3 + 54.8793 v_1^4 u^2 + 54.8793 v_2^4 u^2 + 7.87236 v_1 v_2^3 u^2 + 4.76209 v_1^2 v_2^2 u^2 \\
& + 7.87236 v_1^3 v_2 u^2 + 7.99517 v_1^5 u + 7.99517 v_2^5 u. \\
& \hspace{12cm} \text{(A3)}
\end{aligned}
$$

[1] C. J. Myatt, E. A. Burt, R. W. Ghrist, E. A. Cornell, and C. E. Wieman, Production of Two Overlapping Bose-Einstein Condensates by Sympathetic Cooling, Phys. Rev. Lett. **78**, 586 (1997).

[2] D. S. Hall, M. R. Matthews, J. R. Ensher, C. E. Wieman, and E. A. Cornell, Dynamics of Component Separation in a Binary Mixture of Bose-Einstein Condensates, Phys. Rev. Lett. **81**, 1539 (1998).

[3] J. Stenger, S. Inouye, D. M. Stamper-Kurn, H.-J. Miesner, A. P. Chikkatur, and W. Ketterle, Spin domains in ground-state Bose-Einstein condensates, Nature (London) **396**, 345 (1998).

[4] H. Miesner, D. M. Stamper-Kurn, J. Stenger, S. Inouye, A. P. Chikkatur, and W. Ketterle, Observation of Metastable States in Spinor Bose-Einstein Condensates, Phys. Rev. Lett. **82**, 2228 (1999).

[5] P. Maddaloni, M. Modugno, C. Fort, F. Minardi, and M. Inguscio, Collective Oscillations of Two Colliding Bose-Einstein Condensates, Phys. Rev. Lett. **85**, 2413 (2000).

[6] G. Delannoy, S. G. Murdoch, V. Boyer, V. Josse, P. Bouyer, and A. Aspect, Understanding the production of dual Bose-Einstein condensation with sympathetic cooling, Phys. Rev. A **63**, 051602 (2001).

[7] G. Ferrari, M. Inguscio, W. Jastrzebski, G. Modugno, G. Roati, and A. Simoni, Collisional Properties of Ultracold K-Rb Mixtures, Phys. Rev. Lett. **89**, 053202 (2002).

[8] G. Modugno, M. Modugno, F. Riboli, G. Roati, and M. Inguscio, Two Atomic Species Superfluid, Phys. Rev. Lett. **89**, 190404 (2002).

[9] K. M. Mertes, J. W. Merrill, R. Carretero-González, D. J. Frantzeskakis, P. G. Kevrekidis, and D. S. Hall, Nonequilibrium Dynamics and Superfluid Ring Excitations in Binary Bose-Einstein Condensates, Phys. Rev. Lett. **99**, 190402 (2007).

[10] G. Roati, M. Zaccanti, C. D'Errico, J. Catani, M. Modugno, A. Simoni, M. Inguscio, and G. Modugno, ^{39}K Bose-Einstein Condensate with Tunable Interactions, Phys. Rev. Lett. **99**, 010403 (2007).

[11] J. Catani, L. De Sarlo, G. Barontini, F. Minardi, and M. Inguscio, Degenerate Bose-Bose mixture in a three-dimensional optical lattice, Phys. Rev. A **77**, 011603(R) (2008).

[12] G. Thalhammer, G. Barontini, L. De Sarlo, J. Catani, F. Minardi, and M. Inguscio, Double Species Bose-Einstein Condensate with Tunable Interspecies Interactions, Phys. Rev. Lett. **100**, 210402 (2008).

[13] S. B. Papp, J. M. Pino, and C. E. Wieman, Tunable Miscibility in a Dual-Species Bose-Einstein Condensate, Phys. Rev. Lett. **101**, 040402 (2008).

[14] T. Fukuhara, S. Sugawa, Y. Takasu, and Y. Takahashi, All-optical formation of quantum degenerate mixtures, Phys. Rev. A **79**, 021601 (2009).

[15] D. M. Weld, P. Medley, H. Miyake, D. Hucul, D. E. Pritchard, and W. Ketterle, Spin Gradient Thermometry for Ultracold Atoms in Optical Lattices, Phys. Rev. Lett. **103**, 245301 (2009).

[16] R. P. Anderson, C. Ticknor, A. I. Sidorov, and B. V. Hall, Spatially inhomogeneous phase evolution of a two-component Bose-Einstein condensate, Phys. Rev. A **80**, 023603 (2009).

[17] B. Gadway, D. Pertot, R. Reimann, and D. Schneble, Superfluidity of Interacting Bosonic Mixtures in Optical Lattices, Phys. Rev. Lett. **105**, 045303 (2010).

[18] S. Tojo, Y. Taguchi, Y. Masuyama, T. Hayashi, H. Saito, and T. Hirano, Controlling phase separation of binary Bose-Einstein condensates via mixed-spin-channel Feshbach resonance, Phys. Rev. A **82**, 033609 (2010).

[19] K. Kasamatsu and M. Tsubota, Static and dynamic properties of multicomponent Bose-Einstein condensates of ytterbium atoms, J. Low Temp. Phys. **150**, 599 (2008).

[20] S. Sugawa, R. Yamazaki, S. Taie, and Y. Takahashi, Bose-Einstein condensate in gases of rare atomic species, Phys. Rev. A **84**, 011610 (2011).

[21] P. Soltan-Panahi, J. Struck, P. Hauke, A. Bick, W. Plenkers, G. Meineke, C. Becker, P. Windpassinger, M. Lewenstein, and K. Sengstock, Multi-component quantum gases in spin-dependent hexagonal lattices, Nat. Phys. **7**, 434 (2011).

[22] P. Soltan-Panahi, D. Lhmann, J. Struck, P. Windpassinger, and K. Sengstock, Quantum phase transition to unconventional multi-orbital superfluidity in optical lattices, Nat. Phys. **8**, 71 (2012).

[23] T.-L. Ho and V. B. Shenoy, Binary Mixtures of Bose Condensates of Alkali Atoms, Phys. Rev. Lett. **77**, 3276 (1996).

[24] M. Boninsegni, Phase Separation in Mixtures of Hard-Core Bosons, Phys. Rev. Lett. **87**, 087201 (2001).

[25] E. Altman, W. Hofstetter, E. Demler, and M. D. Lukin, Phase diagram of two-component bosons on an optical lattice, New J. Phys. **5**, 113 (2003).

[26] L.-M. Duan, E. Demler, and M. D. Lukin, Controlling Spin Exchange Interactions of Ultracold Atoms in Optical Lattices, Phys. Rev. Lett. **91**, 090402 (2003).

[27] A. B. Kuklov and B. V. Svistunov, Counterflow Superfluidity of Two-Species Ultracold Atoms in a Commensurate Optical Lattice, Phys. Rev. Lett. **90**, 100401 (2003).

[28] B. Paredes and J. I. Cirac, From Cooper Pairs to Luttinger Liquids with Bosonic Atoms in Optical Lattices, Phys. Rev. Lett. **90**, 150402 (2003).

[29] K. V. Krutitsky and R. Graham, Spin-1 bosons with coupled ground states in optical lattices, Phys. Rev. A **70**, 063610 (2004).

[30] A. B. Kuklov, N. Prokof'ev, and B. V. Svistunov, Superfluid-Superfluid Phase Transitions in a Two-Component Bose-Einstein Condensate, Phys. Rev. Lett. **92**, 030403 (2004).

[31] A. Isacsson, M.-C. Cha, K. Sengupta, and S. M. Girvin, Superfluid-insulator transitions of two-species bosons in an optical lattice, Phys. Rev. B **72**, 184507 (2005).

[32] R. V. Pai, K. Sheshadri, and R. Pandit, Phases and transitions in the spin-1 Bose-Hubbard model: Systematics of a mean-field theory, Phys. Rev. B **77**, 014503 (2008).

[33] S. G. Söyler, B. Capogrosso-Sansone, N. V. Prokof'ev, and B. V. Svistunov, Sign-alternating interaction mediated by strongly correlated lattice bosons, New J. Phys. **11**, 073036 (2009).

[34] A. Hubener, M. Snoek, and W. Hofstetter, Magnetic phases of two-component ultracold bosons in an optical lattice, Phys. Rev. B **80**, 245109 (2009).

[35] B. Capogrosso-Sansone, S. G. Söyler, N. V. Prokof'ev, and B. V. Svistunov, Critical entropies for magnetic ordering in bosonic mixtures on a lattice, Phys. Rev. A **81**, 053622 (2010).

[36] L. de Forges de Parny, F. Hébert, V. G. Rousseau, R. T. Scalettar, and G. G. Batrouni, Ground state phase diagram of spin-1/2 bosons in a two-dimensional optical lattice, Phys. Rev. B **84**, 064529 (2011).

[37] P. Facchi, G. Florio, S. Pascazio, and F. V. Pepe, Binary mixtures of condensates in generic confining potentials, J. Phys. A **44**, 505305 (2011).

[38] L. Pollet, Recent developments in quantum Monte-Carlo simulations with applications for cold gases, Rep. Prog. Phys. **75**, 094501 (2012).

[39] F. V. Pepe, P. Facchi, G. Florio, and S. Pascazio, Domain wall suppression in trapped mixtures of Bose-Einstein condensates, Phys. Rev. A **86**, 023629 (2012).

[40] A. Angelone, M. Campostrini, and E. Vicari, Universal quantum behaviors of interacting fermions in 1D traps: From few particles to the trap thermodynamic limit, Phys. Rev. A **89**, 023635 (2014).

[41] J.-P. Lv, Q.-H. Chen, and Y. Deng, Two-species hard-core bosons on the triangular lattice: A quantum Monte Carlo study, Phys. Rev. A **89**, 013628 (2014).

[42] A. Roy, S. Gautam, and D. Angom, Goldstone modes and bifurcations in phase-separated binary condensates at finite temperature, Phys. Rev. A **89**, 013617 (2014).

[43] M. A. García-March, B. Juliá-Díaz, G. E. Astrakharchik, Th. Busch, J. Boronat, and A. Polls, Quantum correlations and spatial localization in one-dimensional ultracold bosonic mixtures, New J. Phys. **16**, 103004 (2014).

[44] P. N. Galteland, E. Babaev, and A. Sudbo, Thermal remixing of phase-separated states in two-component bosonic condensates, New J. Phys. **17**, 103040 (2015).

[45] P. N. Galteland, E. Babaev, and A. Sudbø, Immiscibile two-component Bose Einstein condensates beyond mean-field approximation: Phase transitions and rotational response, arXiv:1503.05583.

[46] A. Sartori, J. Marino, S. Stringari, and A. Recati, Spin dipole oscillation and relaxation of coherently coupled Bose-Einstein condensates, New J. Phys. **17**, 093036 (2015).

[47] K. Suthar, A. Roy, and D. Angom, Fluctuation-driven topological transition of binary condensates in optical lattices, Phys. Rev. A **91**, 043615 (2015).

[48] A. Roy and D. Angom, Thermal suppression of phase separation in condensate mixtures, Phys. Rev. A **92**, 011601(R) (2015).

[49] F. Lingua, B. Capogrosso-Sansone, M. Guglielmino, and V. Penna, Demixing effects in mixtures of two bosonic species, Phys. Rev. A **92**, 053610 (2015).

[50] G. Ceccarelli, J. Nespolo, A. Pelissetto, and E. Vicari, Bose-Einstein condensation and critical behavior of two-component bosonic gases, Phys. Rev. A **92**, 043613 (2015).

[51] I. Bloch, J. Dalibard, and W. Zwerger, Many-body physics with ultracold gases, Rev. Mod. Phys. **80**, 885 (2008).

[52] B. Capogrosso-Sansone, N. V. Prokof'ev, and B. V. Svistunov, Phase diagram and thermodynamics of the three-dimensional Bose-Hubbard model, Phys. Rev. B **75**, 134302 (2007).

[53] J. Carrasquilla and M. Rigol, Superfluid to normal phase transition in strongly correlated bosons in two and three dimensions, Phys. Rev. A **86**, 043629 (2012).

[54] G. Ceccarelli, C. Torrero, and E. Vicari, Critical parameters from trap-size scaling in trapped particle systems, Phys. Rev. B **87**, 024513 (2013).

[55] G. Ceccarelli and J. Nespolo, Universal scaling of three-dimensional bosonic gases in a trapping potential, Phys. Rev. B **89**, 054504 (2014).

[56] J. A. Lipa, D. R. Swanson, J. A. Nissen, T. C. P. Chui, and U. E. Israelsson, Heat Capacity and Thermal Relaxation of Bulk Helium Very Near the Lambda Point, Phys. Rev. Lett. **76**, 944 (1996).

[57] M. Campostrini, M. Hasenbusch, A. Pelissetto, and E. Vicari, Theoretical estimates of the critical exponents of the superfluid transition in ⁴He by lattice methods, Phys. Rev. B **74**, 144506 (2006).

[58] A. Pelissetto and E. Vicari, Critical phenomena and renormalization-group theory, Phys. Rep. **368**, 549 (2002).

[59] The MF Hamiltonian (4) is in general an infinite-dimensional matrix so that, to obtain numerical results, one must fix a cutoff on the site occupancy. We fix both occupation numbers of the two species to be at most $N_{\max}$ so that (4) becomes a $(N_{\max} + 1)^2 \times (N_{\max} + 1)^2$ real symmetric matrix. Of course, the cutoff is arbitrary and may induce a bias in MF calculations. For this reason, the stability of the results must be checked *a posteriori*, repeating the computation for increasing values of $N_{\max}$. Note that, in the HC limit, no truncation is needed and the MF Hamiltonian is simply a 4×4 matrix.

[60] A. W. Sandvik and J. Kurlijärvi, Quantum Monte Carlo simulation method for spin systems, Phys. Rev. B **43**, 5950 (1991).

[61] O. F. Syljuåsen and A. W. Sandvik, Quantum Monte Carlo with directed loops, Phys. Rev. E **66**, 046701 (2002).

[62] K.-S. Liu and M. E. Fisher, Quantum lattice gas and the existence of a supersolid, J. Low Temp. Phys. **10**, 655 (1973).

[63] M. E. Fisher and D. R. Nelson, Spin Flop, Supersolids, and Bicritical and Tetracritical Points, Phys. Rev. Lett. **32**, 1350 (1974).

[64] D. R. Nelson, J. M. Kosterlitz, and M. E. Fisher, Renormalization-Group Analysis of Bicritical and Tetracritical Points, Phys. Rev. Lett. **33**, 813 (1974).

[65] J. M. Kosterlitz, D. R. Nelson, and M. E. Fisher, Bicritical and tetracritical points in anisotropic antiferromagnetic systems, Phys. Rev. B **13**, 412 (1976).

[66] G. Grinstein and J. Toner, Dislocation-Loop Theory of the Nematic-Smectic *A*-Smectic *C* multicritical point, Phys. Rev. Lett. **51**, 2386 (1983).

[67] D. H. Lee, G. Grinstein, and J. Toner, Commensurate and Incommensurate Vortices in Two-Dimensional XY Models, Phys. Rev. Lett. **56**, 2318 (1986).

[68] S.-C. Zhang, A unified theory based on SO(5) symmetry of superconductivity and antiferromagnetism, Science **275**, 1089 (1997); S.-C. Zhang, J.-P. Hu, E. Arrigoni, W. Hanke, and A. Auerbach, Projected SO(5) models, Phys. Rev. B **60**, 13070 (1999).

[69] A. Aharony, Comment on Bicritical and Tetracritical Phenomena and Scaling Properties of the SO(5) Theory, Phys. Rev. Lett. **88**, 059703 (2002).

[70] A. Aharony, Old and new results on multicritical points, J. Stat. Phys. **110**, 659 (2003).

[71] P. Calabrese, A. Pelissetto, and E. Vicari, Multicritical behavior of O(n_1) ⊕ O(n_2)-symmetric systems, Phys. Rev. B **67**, 054505 (2003).

[72] M. Hasenbusch, A. Pelissetto, and E. Vicari, Instability of O(5) multicritical behavior in SO(5) theory of high-T_c superconductors, Phys. Rev. B **72**, 014532 (2005).

[73] P. Calabrese, A. Pelissetto, and E. Vicari, Multicritical behavior in frustrated spin systems with noncollinear order, Nucl. Phys. B **709**, 550 (2005).

[74] A. Pelissetto and E. Vicari, Interacting N-vector order parameters with O(N) symmetry, Condens. Matter Phys. (Ukraine) **8**, 87 (2005).

[75] M. Holtschneider and W. Selke, Biconical structures in two-dimensional anisotropic Heisenberg antiferromagnets, Phys. Rev. B **76**, 220405 (2007).

[76] A. Pelissetto and E. Vicari, Multicritical behavior of two-dimensional anisotropic antiferromagnets in a magnetic field, Phys. Rev. B **76**, 024436 (2007).

[77] M. Hasenbusch, F. Parisen Toldin, A. Pelissetto, and E. Vicari, Magnetic-glassy multicritical behavior of 3D $\pm J$ Ising model, Phys. Rev. B **76**, 184202 (2007); Multicritical Nishimori point in the phase diagram of the $\pm J$ Ising model on the square lattice, Phys. Rev. E **77**, 051115 (2008).

[78] G. 't Hooft and M. J. G. Veltman, Regularization and renormalization of gauge fields, Nucl. Phys. B **44**, 189 (1972).

[79] R. Schloms and V. Dohm, Minimal renormalization without ϵ-expansion: Critical behavior in three dimensions, Nucl. Phys. B **328**, 639 (1989).

[80] J. Zinn-Justin, *Quantum Field Theory and Critical Phenomena*, 4th ed. (Clarendon, Oxford, 2002).

[81] K. G. Wilson and M. E. Fisher, Critical Exponents In 3.99 Dimensions, Phys. Rev. Lett. **28**, 240 (1972).

[82] A. Aharony, in *Phase Transitions and Critical Phenomena*, edited by C. Domb and M. S. Green (Academic Press, New York, 1976),Vol. 6, p. 357.

[83] B. I. Halperin, T. C. Lubensky, and S. K. Ma, First-Order Phase Transitions in Superconductors and Smectic-A Liquid Crystals, Phys. Rev. Lett. **32**, 292 (1974).

[84] S. Mo, J. Hove, and A. Sudbø, Order of the metal-to-superconductor transition, Phys. Rev. B **65**, 104501 (2002).

[85] F. S. Nogueira and H. Kleinert, in *Order, Disorder, and Criticality*, edited by Y. Holovatch (World Scientific, Singapore, 2007).

[86] C. W. Garland and G. Nounesis, Critical behavior at nematic–smectic-A phase transitions, Phys. Rev. E **49**, 2964 (1994).

[87] P. Calabrese, P. Parruccini, A. Pelissetto, and E. Vicari, Critical behavior of O(2)$\otimes$ O(N)-symmetric models, Phys. Rev. B **70**, 174439 (2004).

[88] Y. Nakayama and T. Ohtsuki, Bootstrapping Phase Transitions in QCD and Frustrated Spin Systems, Phys. Rev. D **91**, 021901 (2015).

[89] M. De Prato, A. Pelissetto, and E. Vicari, Normal-to-planar superfluid transition in He^3, Phys. Rev. B **70**, 214519 (2004).

[90] H. Kawamura, Renormalization-group analysis of chiral transitions, Phys. Rev. B **38**, 4916 (1988).

[91] A. Pelissetto, P. Rossi, and E. Vicari, The critical behavior of frustrated spin models with noncollinear order, Phys. Rev. B **63**, 140414(R) (2001).

[92] M. Hasenbusch and E. Vicari, Anisotropic perturbations in three-dimensional O(N)-symmetric vector models, Phys. Rev. B **84**, 125136 (2011).

[93] M. Hasenbusch, Eliminating leading corrections to scaling in the three-dimensional $O(N)$-symmetric ϕ^4 model: $N = 3$ and 4, J. Phys. A **34**, 8221 (2001).

[94] I. M. Georgescu, S. Ashhab and F. Nori, Quantum simulation, Rev. Mod. Phys. **86**, 153 (2014).

[95] N. Navon, A. L. Gaunt, R. P. Smith, and Z. Hadzibabic, Critical dynamics of spontaneous symmetry breaking in a homogeneous Bose gas, Science **347**, 167 (2015).

[96] M. Campostrini and E. Vicari, Critical Behavior and Scaling in Trapped Systems, Phys. Rev. Lett. **102**, 240601 (2009); **103**, 269901(E) (2009); Trap-size scaling in confined particle systems at quantum transitions, Phys. Rev. A **81**, 023606 (2010).